IOP Publishing | Superconductor Science and Technology

Supercond. Sci. Technol. **28** (2015) 105004 (7pp) | doi:10.1088/0953-2048/28/10/105004

Trapped field properties of a concentric-circled MgB_2 bulk composite magnetized by pulsed field and field cooling

H Mochizuki[1], H Fujishiro[1], T Naito[1], A F Albisetti[2] and G Giunchi[3]

[1] Department of Materials Science and Engineering, Faculty of Engineering, Iwate University, 4-3-5 Ueda, Morioka 020-8551, Japan
[2] EDISON S.p.A., Foro Buonaparte 31, 20121 Milano, Italy
[3] Materials Science Consultant, via Teodosio 8, 20131 Milano, Italy

E-mail: fujishiro@iwate-u.ac.jp

Received 11 May 2015, revised 5 July 2015
Accepted for publication 21 July 2015
Published 24 August 2015

Abstract

We investigated the trapped field properties of the concentric-circled MgB_2 bulk composite disk by pulsed field magnetization (PFM), which consists of 36 MgB_2 thin rings for both surfaces of the disk and a small MgB_2 central cylinder in the stainless steel disk. MgB_2 parts were fabricated by a reactive Mg-liquid infiltration (Mg-RLI) method. The trapped field profile just above the composite surface was very concentric circled, which suggested that the superconducting current flows along the azimuthal direction in the MgB_2 rings and the cylinder independently, even though the magnetic flux dynamically moves in the composite during PFM. The trapped field properties by PFM were reproduced qualitatively by the numerical simulation using the critical current density $J_c(B)$ of the MgB_2 parts estimated by the trapped field B_z by the field-cooled magnetization (FCM). The composite disk is a promising candidate to realize the MgB_2 bulk magnet with concentric-circled trapped field distribution magnetized by PFM.

Keywords: MgB_2, trapped field, numerical simulation, critical current density

(Some figures may appear in colour only in the online journal)

1. Introduction

A superconducting bulk magnet using REBaCuO (RE: rare earth element or Y) is one of the typical models for practical applications, such as nuclear magnetic resonance (NMR), magnetic separation, drug delivery systems, and so on [1], which produces quasi-permanent magnets on the order of several tesla. The superconducting properties such as the trapped field B_z and critical current density $J_c(B)$ have been recently enhanced. The long-standing world record field generated by an arrangement of two YBaCuO bulks of $B_z = 17.24$ T at 29 K [2] was recently exceeded by $B_z = 17.6$ T at 26 K in the GdBaCuO bulk pair by improving the mechanical strength [3]. Some approaches to enhance the B_z and J_c have been performed such as the enlargement of diameter in the bulk disk and the introduction of new pinning centers [4, 5]. It is customary to fabricate the REBaCuO bulk with controlled melt processing of a top-seeded melt growth (TSMG) using a NdBaCuO or SmBaCuO (001) seed crystal, in which a highly textured structure with its *c*-axis oriented perpendicular to the bulk surface can be fabricated. In the TSMG method, however, four-fold growth sector boundaries (GSBs) exist essentially in the *a*-growth region, in which the J_c value is higher than that in the growth sector regions (GSRs) because of the introduction of pinning centers related with crystal defects, etc. As a result, the trapped field profile also shows four-fold symmetry, which is essentially inevitable and is a disadvantage for the application to the NMR bulk magnet necessary with space uniformity of magnetic field with ppm order [6]. The trapped field inhomogeneity is enhanced for the REBaCuO bulk by the PFM rather than the FCM [7]. The magnetic flux dynamically moves in the bulk with a large temperature rise during the PFM process and the trapped field profile is sensitive to the local $J_c(B, T)$

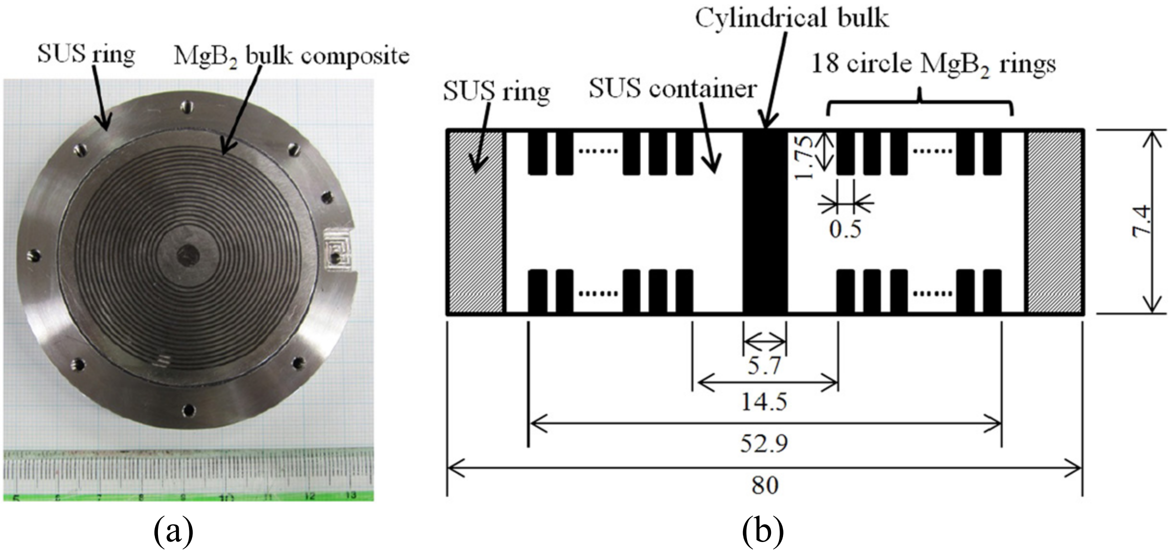

Figure 1. (a) Photograph and (b) schematic view of the cross section of the concentric-circled MgB_2 bulk composite.

distribution in the bulk. Recently, Morita *et al* proposed a new REBaCuO bulk module, in which several thin bulk plates with concentric-circled slits were stacked in order to restrict the supercurrent only in the superconducting slit rings [8]. Sekino *et al* investigated the circumferential inhomogeneity of the trapped field of the bulk composite by FCM [9], in which the trapped field profiles are fairly concentric circled and the slits have the effect of suppressing the distortion of superconducting currents.

On the other hand, better and larger polycrystalline MgB_2 bulk magnets can be recently achieved below the transition temperature $T_c = 39$ K, since the problem of weak links at the grain boundaries can be ignored due to their long coherence length, ξ [10]. MgB_2 bulk magnets are expected for the NMR application because the inhomogeneity of the trapped field profile can be avoided essentially. Several groups have fabricated MgB_2 bulks using different techniques by *in situ* or *ex situ* methods, and reported the trapped field using FCM and PFM. $B_z = 5.4$ T at 12 K was achieved by FCM on a single MgB_2 bulk disk with 20 mm diameter fabricated by hot-pressing ball-milled Mg and B powders [11], which is a record high trapped field on the MgB_2 bulk by FCM to date. Yamamoto *et al* reported that the concentric-circled trapped field profile with a maximum B_z of 1.0 T was realized by FCM, 3 mm above the MgB_2 bulk (30 mm in diameter and 10 mm in thickness) fabricated by *in situ* method [12]. As the trapped field profile by FCM is usually measured on the vacuum sheath, which is $3 \sim 4$ mm above the bulk surface, fine special trapped field distribution might be blurred. It is necessary to scan the profile just above the bulk surface in order to investigate the inhomogeneity of the trapped field and J_c.

Giunchi [13] developed MgB_2 bulks using the reactive Mg-liquid infiltration (Mg-RLI) technique, which is preferable to fabricate dense and large MgB_2 bulk with any form, such as disks, cylinders, rings and so on, where the maximum B_z value was about 1.3 T at 15 K by FCM on the MgB_2 bulk with 55 mm diameter and 15 mm thickness at the center hole of 6 mm. We magnetized the Mg-RLI MgB_2 bulk by PFM and measured the trapped field profile 1 mm above the bulk surface, where the precise trapped field inhomogeneity can be measured [14, 15]. However, the trapped field profile on the MgB_2 polycrystalline bulk magnetized by PFM is not necessarily concentric circled, even though the profile by FCM is nearly conical shaped. Using the Mg-RLI technique, a concentric-circled MgB_2 bulk module was fabricated [16, 17] and we can investigate the trapped field profile on the module magnetized by PFM just above the surface, in which the concentric-circled trapped field profile can be expected.

In this paper, we investigated the trapped field properties of the concentric-circled MgB_2 bulk composite by PFM experimentally and numerically, which consists of 36 MgB_2 rings and a small MgB_2 central cylinder grooved in the stainless substrate.

2. Experimental setup

Figures 1(a) and (b) show the photograph and schematic view of the cross section of the concentric-circled MgB_2 bulk composite used in this study. The MgB_2 parts, which consist of 36 thin rings with slightly different diameter (0.5 mm in width and 1.75 mm in thickness) in both surfaces and a central cylinder (5.7 mm in diameter), were fabricated by Mg-RLI method in the stainless steel (SUS) substrate 61 mm in diameter and 7.4 mm in thickness. The fabrication process of the disk composite is described elsewhere in detail [16, 17].

The experimental setup for PFM is presented in figure 2. The detailed experimental apparatus for PFM is shown elsewhere in detail [15]. The bulk composite mounted in a stainless steel ring was tightly connected on the cold stage of a Gifford–McMahon cycle helium refrigerator. The initial temperature T_s of the composite was set to 15 or 20 K. A magnetizing solenoid coil (94 mm i.d., 153 mm o.d., and

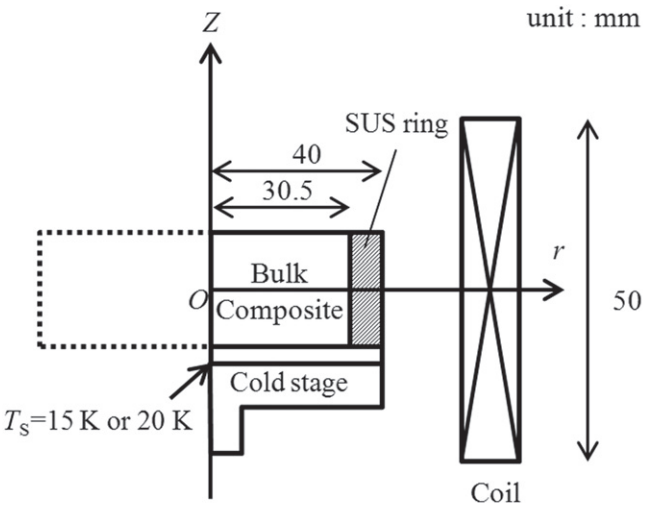

Figure 2. Schematic view of the experimental setup for PFM.

50 mm height), which was dipped in liquid nitrogen, was placed outside the vacuum chamber. A magnetic pulse $B_{ex}(t)$ with a rise time of 0.013 s and a duration time of 0.15 s was applied to the composite with $B_{ex} = 0.8$ to 2.0 T by flowing the pulsed current from a condenser bank. The time evolutions of the local field $B_L{}^C(t)(z = 0\ \mathrm{mm})$ and the final trapped field $B_z(z = 0\ \mathrm{mm})$ were measured by the axial-type Hall sensors (F W Bell, BHA 921) attached on the center of the composite surface using a digital oscilloscope. The two-dimensional trapped field profile $B_z(z = 1\ \mathrm{mm})$ was mapped 1.0 mm above the bulk surface, stepwise with a pitch of 1.0 mm by scanning the same axial-type Hall sensor inside the vacuum chamber using an x–y stage controller with a flexible bellows. Time dependence of temperature $T(t)$ during PFM was monitored by a Cernox thermometer connected to the outer stainless steel ring by a screw.

FCM was also performed for the bulk composite. A static magnetic field of $B_{ex} = 5$ T was applied to the composite above T_c using a cryo-cooled superconducting solenoid magnet (JASTEC JMTD-10T100) and then the composite was field-cooled to T_s. Afterwards, the applied field was decreased down to zero at a rate of $-0.22\ \mathrm{T\ min^{-1}}$. The temperature dependence of the trapped field by FCM $B_z^{FCM}(T)$ $(z = 0\ \mathrm{mm})$ was measured by a 'sweep method,' that is, after the FCM procedure at T_s, the composite was warmed slowly with a heating rate of $0.1\ \mathrm{K\ min^{-1}}$. The $B_z^{FCM}(T)(z = 0\ \mathrm{mm})$ values were measured using three Hall sensors (AREPOC s.r.o., LHP-NP) adhered on the composite surface at the center $(x = 0\ \mathrm{mm})$, and at the positions of $x = 4.5$ and 5.5 mm. The $B_z^{FCM}(T)(z = 0\ \mathrm{mm})$ was also measured for the MgB_2 bulk disk (54 mm in diameter and 15 mm in thickness), which was fabricated by the same Mg-RLI method [15], in order to estimate the critical current density $J_c(B)$ of the MgB_2 parts in the composite for the numerical simulation. After the FCM experiments, the MgB_2 bulk disk was cut, and a small piece about $1 \times 1 \times 2\ \mathrm{mm}^3$ in size was prepared and the magnetization curve $M(H)$ was measured at 20 K under a magnetic field up to $\mu_0 H = 5$ T using a commercial SQUID magnetometer (MPMS-5 T; Quantum Design). The J_c-B relationship was estimated using the extended Bean model [18], $J_c = 20\Delta M/a(1\text{-}a/3b)$, where a and b are the dimensions of the plane of the sample perpendicular to the applied field and ΔM is the width of the $M(H)$ hysteresis loop.

3. Numerical model of analysis

Based on the experimental setup, the framework for the numerical simulation for both PFM and FCM was constructed, in which the physical phenomena occurring during the magnetization processes are described using the fundamental electromagnetic and thermal equations in axisymmetric coordinates. The detail of the numerical simulation was described elsewhere [19, 20]. Briefly, the power-n model ($n = 100$) was used to describe the nonlinear E–J characteristic of the MgB_2 part. The measured $J_c(B)$ of the MgB_2 disk at 20 K was fitted using the following equation,

$$J_c(B) = J_{c0}\exp\left[-\left(\frac{B}{B_0}\right)^{\beta}\right], \tag{1}$$

where B_0 and β are the fitting parameters. The temperature dependence of the critical current density J_{c0} under the zero field is described by the following equation [19],

$$J_{c0} = \alpha\left\{1 - \left(\frac{T}{T_c}\right)^2\right\}^{3/2}, \tag{2}$$

where T_c is the critical temperature and α is a constant representing J_c at 0 K. In order to reproduce the trapped field properties of the composite disk, J_c–B characteristics of the MgB_2 parts were estimated according to equations (1) and (2).

Iterative calculations were performed to analyze the combined problem of electromagnetic fields and heat diffusion using the finite element method (FEM) using commercial software, Photo-Eddy, combined with Photo-Thermo (Photon Ltd, Japan). In the model analysis of FEM, the bulk composite was equally divided with 0.25 mm mesh and temperature dependence of thermal conductivity $\kappa(T)$ and the specific heat $C(T)$ of the MgB_2 and stainless steel were introduced in the analysis [21, 22].

4. Experimental results

4.1. PFM

Figure 3 shows the pulsed field dependence of the trapped field B_z^{PFM} $(z = 0\ \mathrm{mm})$ at the center of the disk composite magnetized by PFM at $T_s = 15$ and 20 K. The result of the MgB_2 bulk disk was also shown [15]. Similarly to the previous experimental results of REBaCuO and MgB_2 bulks [15, 23], the $B_z^{PFM}(z = 0\ \mathrm{mm})$ value increases, takes a maximum and then decreases with increasing B_{ex}. The maximum $B_z^{PFM}(z = 0\ \mathrm{mm})$ was slightly increased and the B_z^{PFM} $(z = 0\ \mathrm{mm})$–B_{ex} relation shifts to higher B_{ex} side with

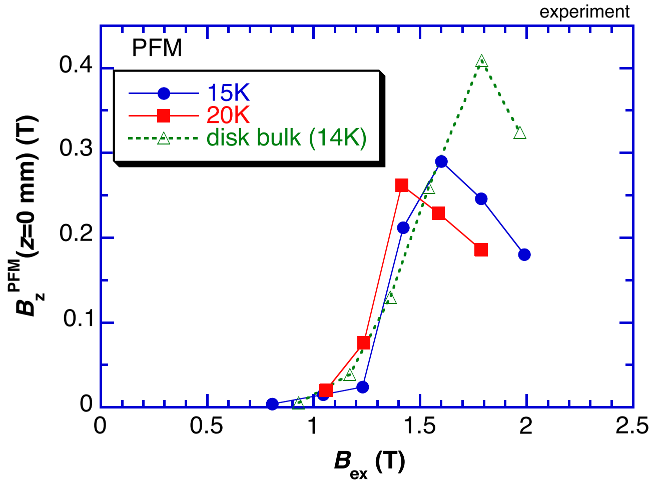

Figure 3. Pulsed field dependence of the trapped field B_z^{PFM} ($z = 0$ mm) at the center of the disk composite magnetized by PFM at $T_s = 15$ and 20 K. The results for the MgB_2 bulk disk at $T_s = 14$ K are also shown [15].

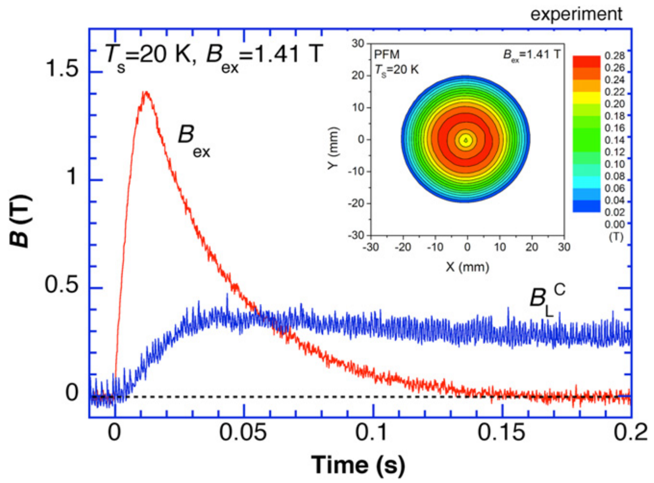

Figure 4. Time evolution of the applied field $B_{ex}(t)$ and the local field $B_L^C(t)$ ($z = 0$ mm) at the center of the surface at 20 K after applying the pulsed field of $B_{ex} = 1.41$ T. The inset shows the trapped field profile B_z^{PFM}($z = 1$ mm) of the disk composite after PFM.

decreasing T_s due to the increase in J_c of the MgB_2 parts. The maximum B_z^{PFM}($z = 0$ mm) was 0.29 T at 15 K, which was smaller than that of the MgB_2 bulk disk at 14 K.

Figure 4 presents the time evolution of the applied field $B_{ex}(t)$ and the local field $B_L^C(t)$($z = 0$ mm) at the center of the surface at 20 K after applying the pulsed field of $B_{ex} = 1.41$ T. $B_L^C(t)$($z = 0$ mm) started to increase with a slight time delay, took a maximum of 0.38 T at 0.04 s, gradually decreased and approached to the final value with the increase in time. The flux jump did not happen in the disk composite under our experimental condition of T_s and B_{ex}, which frequently takes place for the MgB_2 bulk disk with higher J_c and for the higher B_{ex} [24]. The inset of figure 4 shows the trapped field profile B_z^{PFM}($z = 1$ mm) of the disk composite 1 mm above the disk surface under the same

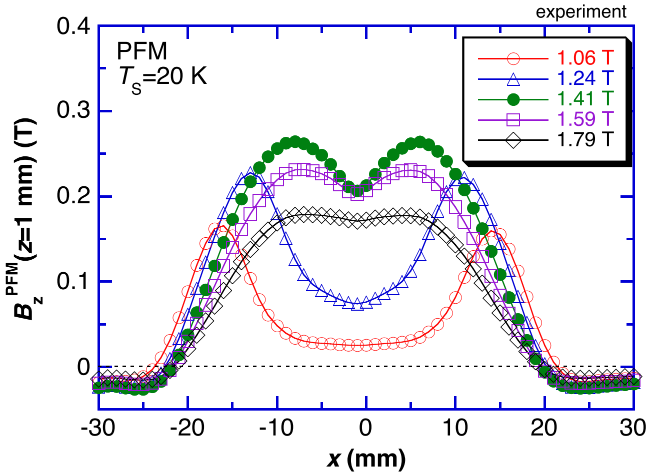

Figure 5. The cross section of the trapped field profile B_z^{PFM} ($z = 1$ mm) for each B_{ex}.

condition. The profile shows fairly concentric circles with a slightly concave profile near the center.

Figure 5 shows the cross section of the trapped field profile B_z^{PFM}($z = 1$ mm) for each B_{ex}. For $B_{ex} = 1.06$ T, the profile was concave and the trapped field increased with increasing B_{ex}. For $B_{ex} = 1.41$ T, the trapped field took a maximum and then decreased with further increase in B_{ex}. The profile is axisymmetric for all the B_{ex}, even just above the bulk surface. The symmetric profile suggests that the superconducting current flows independently along the azimuthal direction in each MgB_2 ring and cylinder. For the MgB_2 bulk disk, the trapped field profile with the concentric circle can be obtained by FCM in principle. However, the trapped field profile of the MgB_2 disk bulk by PFM did not necessarily show the concentric-circled one [14]. Using this bulk composite, the concentric-circled profile can be realized even by PFM. It should be noted that the profile is not completely conical but concave or trapezoidal for all the applied fields. The reason is discussed later. However, from the viewpoint of the concentric-circled profile, this type of the composite can be applicable for NMR magnetized by PFM, in which the trapped field homogeneity is quite severe [6].

Figure 6(a) presents the time evolution of temperature $T(t)$ during PFM in the disk composite at $T_s = 20$ K for various applied pulsed fields. For each B_{ex}, temperature rose sharply within several seconds, which increased with increasing B_{ex}, and then decreased and quickly recovered to the initial temperature T_s with several hundred seconds. The quick response in $T(t)$ is similar to that of the MgB_2 bulk disk [15] and comes from the low specific heat $C(T)$ and high thermal conductivity $\kappa(T)$, which is clearly in contrast with those of the REBCO bulk [25]. Figure 6(b) presents the maximum temperature rise ΔT_{max} at $T_s = 15$ and 20 K a$_s$ a function of B_{ex}. The ΔT_{max} for the MgB_2 disk bulk at 14 K is also shown [15]. ΔT_{max} increases with increasing applied field B_{ex} for all the cases and becomes small in case of the increase in T_s, which is independent of the structure of the bulk, i.e., a concentric-circled bulk composite or a disk bulk.

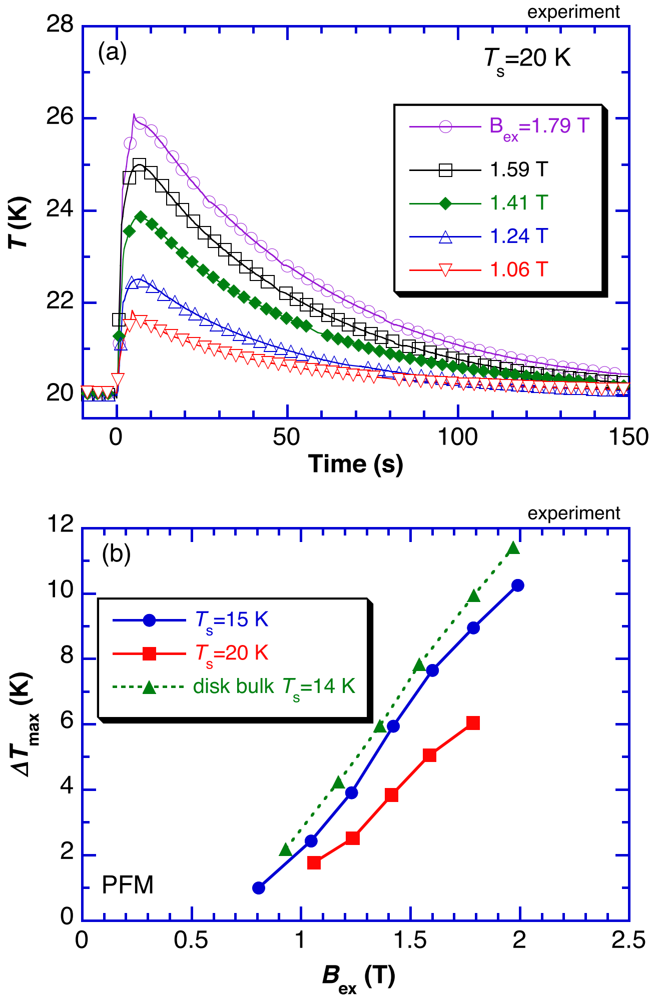

Figure 6. (a) Time dependence of temperature $T(t)$ during PFM in the disk composite at $T_s = 20$ K for various applied pulsed fields B_{ex}. (b) The maximum temperature rise ΔT_{max} at $T_s = 15$ and 20 K as a function of B_{ex}.

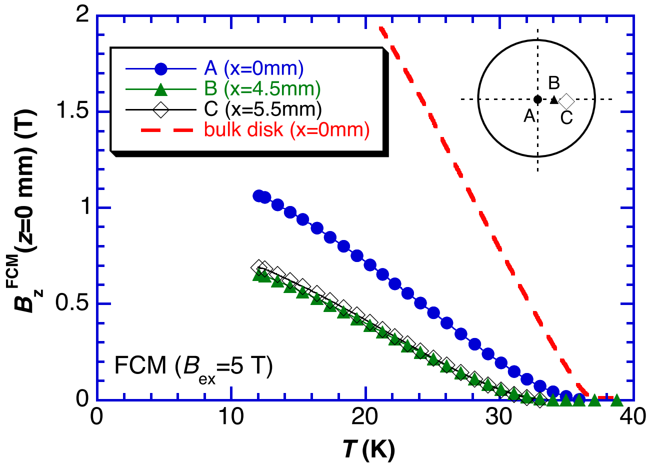

Figure 7. Temperature dependence of the trapped field B_z^{FCM} ($z = 0$ mm) at three positions; A (center, $x = 0$ mm), B ($x = 4.5$ mm), and C ($x = 5.5$ mm) of the composite. B_z^{FCM} ($z = 0$ mm) of the MgB_2 bulk disk at the center is also shown.

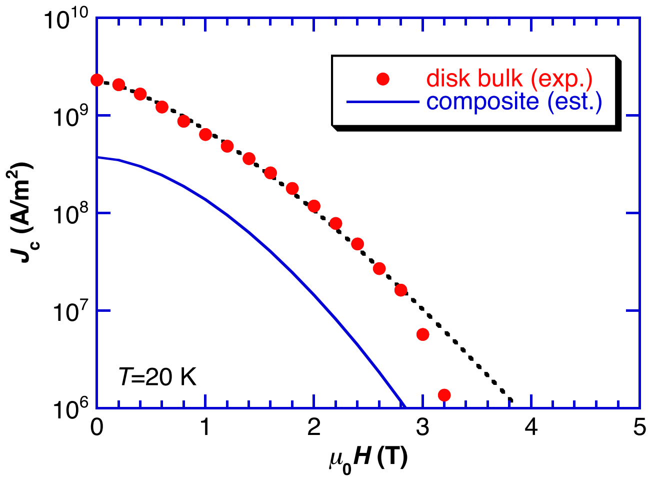

Figure 8. Magnetic field dependence of the critical current density $J_c(B)$ at 20 K for the disk bulk. The fitting curve (dashed line) and the estimated $J_c(B)$ of the MgB_2 part in the composite are also shown (see text).

4.2. FCM

In order to estimate the J_c–B characteristics of the MgB_2 parts in the disk composite, FCM was performed. Figure 7 shows the temperature dependence of the trapped field B_z^{FCM} ($z = 0$ mm) at three positions; A (center, $x = 0$ mm), B ($x = 4.5$ mm), and C ($x = 5.5$ mm), as shown in the inset. In the figure, B_z^{FCM}($z = 0$ mm) at the center of the MgB_2 bulk disk is also shown for comparison. The maximum values of B_z^{FCM}($z = 0$ mm) at 12.1 K are 1.06 T ($x = 0$ mm), 0.65 T ($x = 4.5$ mm), and 0.69 T ($x = 5.5$ mm), respectively. The T_c value decided by the zero field trap was relatively low; $T_c = 36$ K for position A and 34 K for positions B and C, which suggests that the superconducting properties of the MgB_2 parts in the composite are a little bit deteriorated. These results may come from the complicated structure of the disk composite with many narrow ridges, in which the immersed boron powder poorly reacted with liquid Mg. It should be noticed that the cross section of the trapped field profile is not fully corn-shaped, but B_z^{FCM}($z = 0$ mm) at the position C is slightly higher than that at the position B. This result comes from the gap of 4.4 mm between the MgB_2 central cylinder and the innermost MgB_2 ring, as shown in figure 1(b). The volume fraction of MgB_2 parts is estimated to be 15% of the total volume of the disk composite. The trapped field B_z^{FCM} ($z = 0$ mm) lower than that of the bulk disk comes from the smaller volume fraction and the lower superconducting characteristics in the MgB_2 parts.

5. Results of numerical simulation and discussion

5.1. Estimation of J_c–B characteristics in the MgB_2 parts using FCM

In order to clarify the trapped field properties of the bulk composite, it is necessary to estimate the J_c–B characteristics in the MgB_2 part. The plots in figure 8 show the magnetic field dependence of the critical current density $J_c(B)$ at 20 K

Table 1. Determined parameters in equations (1) and (2) for the J_c–B characteristics.

	α (A m^{-2})	B_0 (T)	β
MgB_2 bulk disk (measured)	3.6e9	0.9	1.4
MgB_2 part in the composite (estimated)	5.9e8	1.0	1.7

for the disk bulk. As can be seen in the typical MgB_2 bulks [26], J_c decreases monotonically with increasing magnetic field, which is nearly the same $J_c(0)$ and magnetic field dependence to the bulk fabricated by Mg-RLI method. Using equations (1) and (2), the fitting parameters were decided as shown in table 1 and the fitting curve is shown in figure 8 by dashed line.

Figure 9 presents the cross section of the trapped field profile $B_z^{FCM}(z = 0\,\text{mm})$ by FCM at 20 K, as a function of the position x. The experimental results obtained in figure 7 are plotted in the figure, in which the plots at $x = -4.5$ and -5.5 mm are the axisymmetric assumptions from $x = +4.5$ and $+5.5$ mm. The dashed line shows the results of the numerical simulation using the $J_c(B)$ obtained from the bulk disk shown in figure 8. It should be noticed that the dashed line is quite larger than the experimental results. These results suggest that the $J_c(B)$ for the MgB_2 parts in the composite is supposed to be lower than that obtained from the bulk disk. So we reversely estimated the $J_c(B)$ for the MgB_2 parts in the composite using the experimentally obtained results. In this estimation, the parameters of α, B_0, and β in equations (1) and (2) were decided as shown in table 1 and the estimated $J_c(B)$ is also shown in figure 8 by a solid line. It is found that the estimated $J_c(B)$ of the MgB_2 parts in the composite is about one order of magnitude smaller than that of the MgB_2 bulk disk. The result of the numerical simulation is also shown in figure 9 by a solid line, which can reproduce the experimental data. In the next subsection, the numerical simulation of the PFM for the composite is shown using the estimated $J_c(B)$ relation of the MgB_2 parts.

5.2. Numerical simulation of trapped field properties by PFM

The numerical simulation of the PFM for the composite was performed using the estimated $J_c(B)$ of the MgB_2 parts shown in figure 8. Figure 10 presents the results of the simulation for the cross section of the trapped field profile $B_z^{PFM}(z = 1\,\text{mm})$ by PFM at 20 K, as a function of applied pulsed field B_{ex}. For B_{ex} lower than 0.6 T, the trapped field profile shows a large concave one, which is nearly consistent with the experimental results shown in figure 5, although the applied field B_{ex} in the simulation is somewhat smaller than that in the experiment. However, for B_{ex} larger than 0.8 T, the magnetic flux intrudes in the central part of the composite and the trapped field at the center of the composite increases with increasing B_{ex}, which is clear contrast to the experimental results; in the experiments, the magnetic flux cannot intrude into the center and the maximum trapped field decreased, even if the B_{ex} value increased.

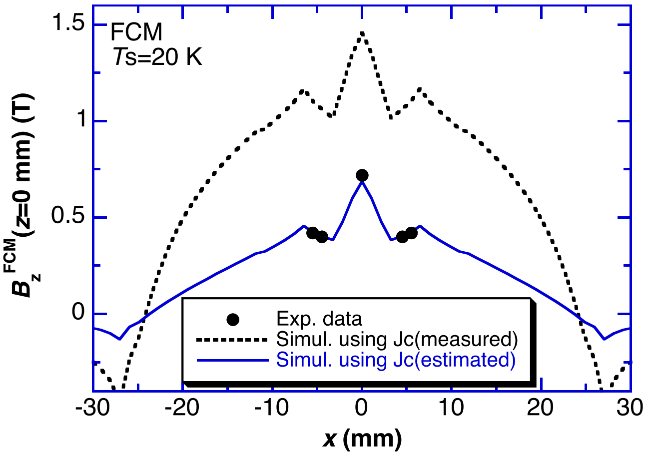

Figure 9. Results of the experiments and numerical simulations of the trapped field profiles for the composite magnetized by FCM (see text).

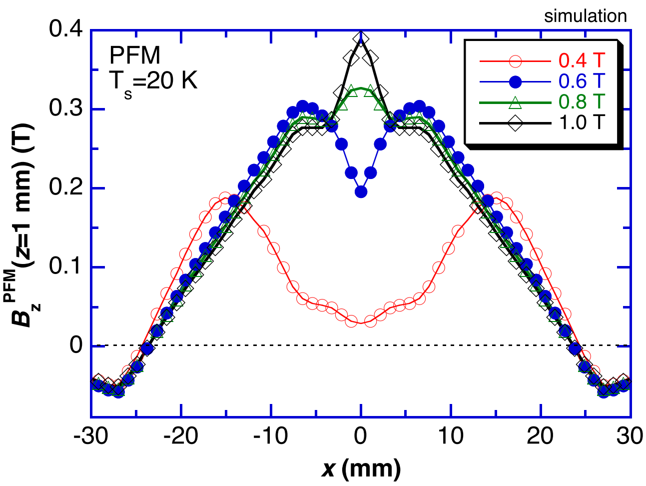

Figure 10. Results of the simulation for the cross section of the trapped field $B_z^{PFM}(z = 1\,\text{mm})$ profile by PFM at 20 K, as a function of applied pulsed field B_{ex}.

The discrepancy between the experiments and simulations may come from several reasons. One possibility is the difference in $J_c(B)$ characteristics for the MgB_2 ring part and the cylinder part; $J_c(B)$ characteristics for the MgB_2 cylinder part may be higher or lower than those for the MgB_2 ring part. For the former case, the MgB_2 cylinder shields the magnetic flux, and for the latter case, the MgB_2 cylinder cannot trap the magnetic flux. However, both hypotheses cannot be realistic because the trapped field profile by FCM can reproduce the experimental results by using identical $J_c(B)$ characteristics for the MgB_2 ring part and the cylinder part, as shown in figure 9. Another possibility is inhomogeneous temperature distribution during PFM. The MgB_2 rings in the bottom were attached directly the cold stage and were cooled. On the other hand, the MgB_2 rings in the upper surface were cooled through the low thermal conductive stainless steel substrate, of which the thermal conductivity $\kappa(T)$ was about one order of magnitude smaller than that of the MgB_2 bulk [25]. The generated heat due to the flux movement and trap in the upper surface are removed through the stainless substrate during PFM. So the temperature on the upper surface can possibly be higher than that on the bottom surface. The thermal contact resistance between each MgB_2 part and the stainless steel substrate may seriously affect the trapped field properties, which was not considered in the numerical simulation. The problem of this discrepancy between figures 5 and 10 remains as a future study.

6. Conclusion

The trapped field properties of the concentric-circled MgB_2 bulk composite disk, which consists of 36 MgB_2 thin rings for both sides of the composite and a MgB_2 central cylinder in the stainless steel substrate and was fabricated by a reactive Mg-RLI method, have been investigated experimentally and numerically. The important results and conclusions obtained from this study are summarized as follows.

(1) The trapped field profile by PFM, $B_z^{\mathrm{PFM}}(z = 1\ \mathrm{mm})$, 1 mm above the disk surface was very concentric circled, which suggested that the superconducting current flows along the azimuthal direction in the MgB_2 rings and the cylinder independently, even though the magnetic flux dynamically moves in the composite during PFM. The trapped field profile is not perfectly conical but slightly concave at the central region.
(2) The critical current density $J_c(B)$ of the MgB_2 parts in the disk composite was estimated using the experimentally obtained trapped field values by FCM and the numerical simulation. The $J_c(B)$ was about one order of magnitude smaller than that of the MgB_2 bulk disk fabricated by the same method.
(3) Using the estimated $J_c(B)$ characteristics of the MgB_2 parts, the numerical simulation for the PFM procedures was performed. For the lower pulsed field region, the trapped field properties were reproduced qualitatively by the numerical simulation.
(4) However, in the simulation, the magnetic flux intruded into the central MgB_2 cylinder for the higher pulsed field region, which is clear contrast to the experimental results. The discrepancy may come from the inhomogeneous temperature distribution due to the existence of the thermal contact resistance between the MgB_2 parts and the stainless steel substrate in the experiment. Detailed analysis remains about the discrepancy in the future study.

Acknowledgments

This work was supported in part by JSPS KAKENHI grant number 23560002 and 15K04646.

References

[1] Oka T 2007 *Physica* C **463–5** 7
[2] Tomita M and Murakami M 2003 *Nature* **421** 517–20
[3] Durrel J H *et al* 2014 *Supercond. Sci. Technol.* **27** 082001
[4] Diko P, Antal V, Kanuchova M, Sefcikova M and Kovac J 2009 *Supercond. Sci. Technol.* **22** 065005
[5] Ishii Y, Shimoyama J, Ogino H and Kishio K 2009 *J. Cryog. Soc. Japan* **44** 573
[6] Nakamura T, Itoh Y, Yoshikawa M, Oka T and Uzawa J 2007 *Concept Mag. Reson.* B (*Mag. Res. Eng.*) **31** 65
[7] Komi Y, Sekino M and Ohsaki H 2009 *Physica* C **469** 1262–5
[8] Morita M and Teshima H 2011 *International Patent Publication Number* WO 2011/071071 A1
[9] Sekino M, Yasuda H, Miyazoe A and Ohsaki H 2011 *IEEE Trans. Appl. Supercond.* **21** 1588–91
[10] Kambara M, Babu N H, Sadki E S, Cooper J R, Minami H, Cardwell D A, Campbell A M and Inoue I H 2001 *Supercond. Sci. Technol.* **14** L5
[11] Fuchs G, Habler W, Nenkov K, Scheiter J, Perner O, Handstein A, Kanai T, Schultz L and Holzapfel B 2013 *Supercond. Sci. Technol.* **26** 122002
[12] Yamamoto A, Ishihara A, Tomita M and Kishio K 2014 *Appl. Phys. Lett.* **105** 032601
[13] Giunchi G, Ceresara S, Ripamonti G, Chiarelli S and Spadoni M 2003 *IEEE Trans. Appl. Supercond.* **13** 3060–3
[14] Fujishiro H, Tamura T, Arayashiki T, Oyama M, Sasaki T, Naito T, Giunchi G and Albisetti A F 2012 *Japan. J. Appl. Phys.* **51** 103005
[15] Fujishiro H, Ujiie T, Naito T, Albisetti A F and Giunchi G 2014 *J. Phys. Conf. Series* **507** 032016
[16] Perini E, Giunchi G, Saglietti L, Albisetti A F, Matrone A and Cavaliere V 2011 *IEEE Trans. Appl. Supercond.* **21** 2690–3
[17] Giunchi G 2011 *IEEE Trans. Appl. Supercond.* **21** 1564–7
[18] Gyorgy E M, van Dover R B, Jackson K A, Schneemeyer L F and Waszczak J V 1989 *Appl. Phys. Lett.* **55** 283–5
[19] Fujisiro H and Naito T 2010 *Supercond. Sci. Technol.* **23** 105021
[20] Fujishiro H, Naito T and Yoshida T 2014 *Supercond. Sci. Technol.* **27** 065019
[21] Sologubenko A V, Jun J, Kazakov S M, Karpinski J and Ott H R 2002 *Phys. Rev.* B **66** 014504
[22] Wang Y, Plackowski T and Junod A 2001 *Physica* C **355** 179–83
[23] Fujishiro H, Hiyama T, Miura T, Naito T, Nariki S, Sakai N and Hirabayashi I 2009 *IEEE Trans. Appl. Supercond.* **19** 3545–8
[24] Fujishiro H, Ujiie T, Mochizuki H, Yoshida T and Naito T 2015 *IEEE Trans. Appl. Supercond.* **23** 6800804
[25] Ainslie M D and Fujishiro H 2015 *Supercond. Sci. Technol.* **28** 053002
[26] Xiang F X, Wang X L, Xun X, Silva K S B, De, Wang Y X and Dou S X 2013 *Appl. Phys. Lett.* **102** 152601